PROCEEDINGS OF SPIE

SPIEDigitalLibrary.org/conference-proceedings-of-spie

Optical stent inspection of surface texture and coating thickness

Carlos Bermudez, Ferran Laguarta, Cristina Cadevall, Aitor Matilla, Sergi Ibañez, et al.

Carlos Bermudez, Ferran Laguarta, Cristina Cadevall, Aitor Matilla, Sergi Ibañez, Roger Artigas, "Optical stent inspection of surface texture and coating thickness," Proc. SPIE 10110, Photonic Instrumentation Engineering IV, 1011007 (20 February 2017); doi: 10.1117/12.2249614

SPIE.

Event: SPIE OPTO, 2017, San Francisco, California, United States

Optical stent inspection of surface texture and coating thickness

Carlos Bermudez*[ab], Ferran Laguarta[a], Cristina Cadevall[ab], Aitor Matilla[b], Sergi Ibañez[c], Roger Artigas[ab]

[a]Center for Sensors, Instruments and Systems Development (CD6), Technical University of Catalonia (UPC), Rambla Sant Nebridi 10, Terrassa, Spain, E-08222; [b]Sensofar-Tech, S.L., Parc Audiovisual de Catalunya, Ctra. BV1274 km 1, Terrassa, Spain E-08225; [c]Sensofar-Medical, S.L., Parc Audiovisual de Catalunya, Ctra. BV1274 km 1, Terrassa, Spain, E-08225

ABSTRACT

Stent quality control is a critical process. Coronary stents have to be inspected 100% so no defective stent is implanted into a human body. We have developed a high numerical aperture optical stent inspection system able to acquire both 2D and 3D images. Combining a rotational stage, an area camera with line-scan capability and a triple illumination arrangement, unrolled sections of the outer, inner, and sidewalls surfaces are obtained with high resolution. During stent inspection, surface roughness and coating thickness uniformity is of high interest. Due to the non-planar shape of the surface of the stents, the thickness values of the coating need to be corrected with the 3D surface local slopes. A theoretical model and a simulation are proposed, and a measurement with white light interferometry is shown. Confocal and spectroscopic reflectometry showed to be limited in this application due to stent surface roughness. Due to the high numerical aperture of the optical system, only certain parts of the stent are in focus, which is a problem for defect detection, specifically on the sidewalls. In order to obtain fully focused 2D images, an extended depth of field algorithm has been implemented. A comparison between pixel variance and Laplacian filtering is shown. To recover the stack image, two different methods are proposed: maximum projection and weighted intensity. Finally, we also discuss the implementation of the processing algorithms in both the CPU and GPU, targeting real-time 2-Million pixel image acquisition at 50 frames per second.

Keywords: stent inspection, machine vision, image processing, optical metrology, thickness

1. INTRODUCTION

Stent manufacturing and implantation has grown exponentially in recent years, and several market researches foresee a continuity of this trend. Stents are miniaturized hollow medical devices made from metallic or polymeric tubes, designed to remove blood restrictions by being expanded through a balloon catheter. Their geometry consists of a mesh of struts specifically designed to perform certain deformations to the vessels and a treated surface to avoid causing any damage to the patient or to the inflation balloon[1]. They are also usually coated with biodegradable drugs to avoid restenosis[2]. To improve the drug release control, new generation stents combine even more than one layer of drug films[3]. Any defect on the struts or unevenness on the coating can reduce its effectiveness or even cause a life-threatening situation. Consequently, quality assurance, which is nowadays carried out by manual visual inspection, is of extreme importance.

Existing stent inspection systems, intended to grant objectivity and repeatability to the inspection process, provide both critical dimension (CD) analysis and defect detection. Nevertheless, they usually produce low-resolution images[4-6] and only few of them have 3D and coating thickness measurement capability, but as a separate subsystem[7]. In this paper we present an optical inspection system that combines a high numerical aperture imaging scheme with a triple-light illumination approach which performs high resolution imaging from the inner and outer surfaces, 3D metrology at the nanometer scale, coating thickness measurement and fully focused microscope images (extended depth of field). The stent is placed on a high-precision rotational stage to obtain complete unrolled images of its surfaces[8]. For those stents with irregular shapes we have also developed a mandrel system that allows imaging the inner surface with high contrast[9]. This system allows for the first time comprehensive optical stent inspection, being able to assess critical dimensions and detect defects using the image modes (conventional or extended depth of field), characterize defects and assess surface texture using the 3D mode, and coating thickness uniformity using the thickness mode.

*bermudez@sensofar.com; phone +34 93 700 14 92; www.sensofar.com

Photonic Instrumentation Engineering IV, edited by Yakov G. Soskind, Craig Olson,
Proc. of SPIE Vol. 10110, 1011007 © 2017 SPIE · CCC code: 0277-786X/17/$18
doi: 10.1117/12.2249614

The remainder of this paper is organized as follows: In Section 2, the design of the stent inspection system will be introduced. Stent 3D surface measurement is proposed in Section 3. Coating thickness measurement is described in Section 4 whereas Section 5 introduces the extended depth of field algorithms and their computing. Finally, conclusions are presented in Section 6.

2. MATERIALS AND METHODS

In order to obtain high lateral resolution, certain numerical aperture needs to be used. However, since stents are of cylindrical shapes, in a bright field microscope with epi-illumination only the light reflected on the area perpendicular to the optical axis returns back to the system, and the rest of the image is out of focus and dark (Figure 1a). A linear Z stage allows focusing the stent in the outer and inner surfaces. We have developed a system that integrates a high precision rotational stage including a backlight LED together with a 2 Million pixel CMOS color camera which can behave both as an area or line scan camera, so we can obtain unrolled sections of the stent at high speed with the line scan mode (Figure 1b). A color camera provides not only more user-friendly images than a monochromatic camera, but also helps with the image segmentation for critical dimensions analysis, combined with a suitable background illumination, in our case green color. The color camera is also suitable for 3D and thickness measurements (see Sections 3 and 4). Finally, a linear stage parallel to the axis of the stent allows moving it axially and acquire all the sections to cover the full area.

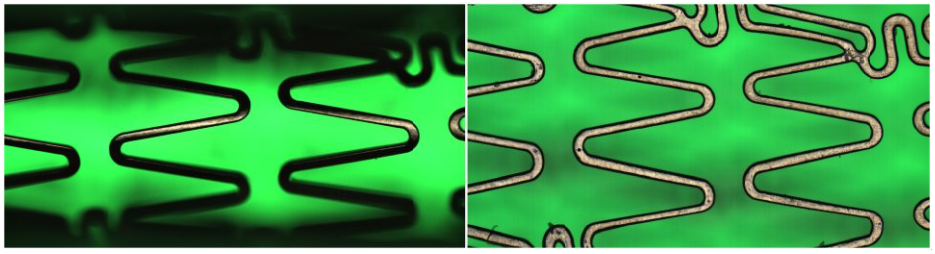

a b

Figure 1. Images obtained with a 5X 0.15NA lens, sampling is 1.76μm. (a) Bright field screenshot, (b) part of a line scan section.

In order to perform 3D surface characterization and coating thickness measurement, we have integrated both confocal[10] and Coherence Scanning Interferometry (CSI)[11]. In Figure 2 we show the sensor head, which integrates a nosepiece with both bright field objectives for imaging and confocal profiling (2.5X to 20X), and Mirau objectives for interferometry (10X-50X). The rest of the sensor head is composed by two illumination branches, one bright field with a white, broadband light source for interferometry and another with a slit spatial filter and a green, narrowband light source used in confocal acquisitions. Both coaxial illumination branches are arranged according to Köhler illumination to maximize light efficiency. Being a reflected light microscope, light coming back to the sensor head is divided to the observation branch.

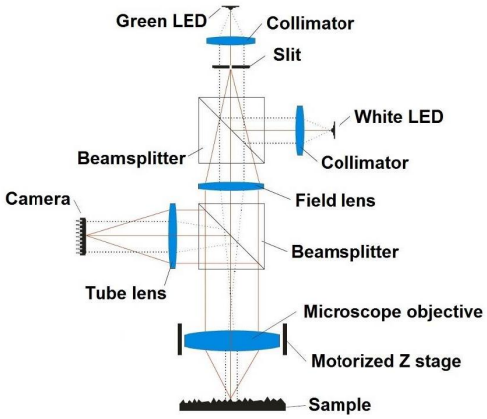

Figure 2. Sensor head optomechanical design. Solid lines represent the image path while dotted lines represent the illumination path.

With respect to the optomechanical design, our confocal approach relies on projecting a set of parallel slits onto the stent surface and obtaining the axial response of the matching pixel row from the camera along a Z scan. We obtain the axial response by recording the camera images and processing them with the classical confocal algorithm or with the gradient calculation.

3. 3D SURFACE PROFILING

The ability to perform 3D measurements is essential in the medical devices field. As it has been pointed out in the introduction, there is currently the need to detect and characterize stent defects and assess surface roughness, because both would affect directly the stent performance once it is implanted into the human body.

The measurement system presented in this paper has adopted CSI as a 3D metrology technique[11]. As described in Section 2, CSI requires a broadband light source, a Mirau interferometric microscope objective and a CMOS camera, which needs to work appropriately with such light spectrum. In order to avoid using a second, monochromatic camera to perform 3D measurements, we have evaluated the use of a color camera for CSI.

3.1 CSI measurement with a color camera

Some research has introduced the use of color cameras for interferometric measurements, by separating the RGB channels to further calculate the phase[12], but this system CSI uses grayscale image, which is obtained from color image.

The CSI technique is based on detecting the envelope maximum position of the correlogram, which is obtained when the sample is scanned vertically so that each point on the surface passes through the focus. Resolution of the topographical measurements depends on the coherence length of the light source. The narrower the coherence envelope peak, the higher the vertical resolution. For this reason the most suitable light sources are continuous spectrum white LEDs or incandescent light bulbs. On the other hand, the numerical aperture of the objective also modifies, to a lesser extent, the envelope width, being narrower with higher NA values.

In order to assess whether the envelope width of the correlogram obtained with a monochrome camera is similar to the one obtained with a color camera, the intensity of one pixel can be recorded along a Z scan. Alternatively, we can take the image (interferogram) of a tilted mirror, obtaining the correlogram intensity as a function of the mirror height in a single shot (Figure 3a & b).

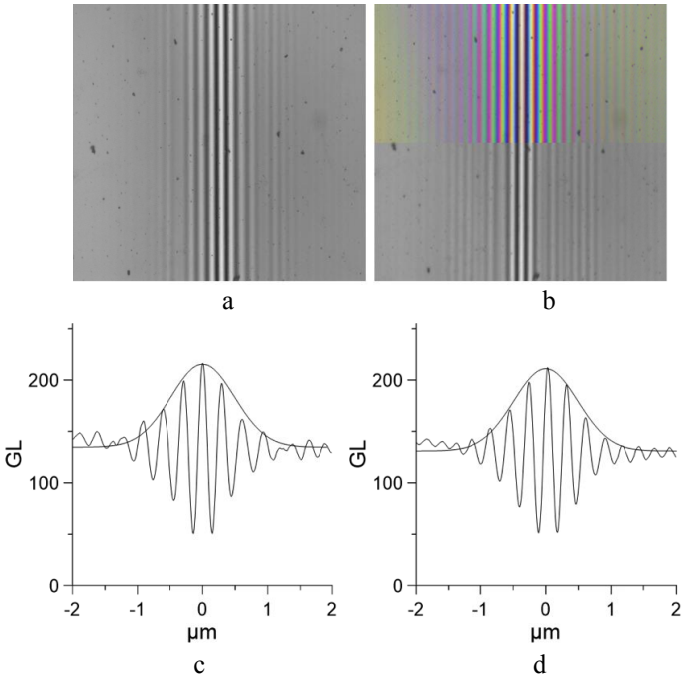

Figure 3. Interferogram of a tilted mirror. (a) Grayscale camera screenshot, (b) color camera screenshot, top part original capture, bottom part transformed to grayscale, (c) intensity of an horizontal profile (correlogram) from (a) with its envelope, (d) idem to (c) but with an intensity profile (correlogram) from (b).

From the images on Figure 3a and b, a horizontal profile (correlogram) has been extracted (Figure 3c and d, respectively). The envelope width has been calculated with an algorithm proposed by Larkin[13].

From such envelopes, we have obtained the Full Width Half Maximum (FWHM), which determines the CSI vertical resolution and repeatability. Table 1 shows the FWHM values from said envelopes. Being the correlogram recorded with the color camera marginally broader than the one obtained with the monochrome camera, we can establish that this setup is valid for CSI measurements in terms of vertical resolution and repeatability. However, color camera would produce slightly lower lateral resolution images due to the Bayer arrangement of color filters on the pixel array.

Table 1. Correlogram envelope FWHM results. Color image produces a slightly broader envelope.

Interferogram envelope	FWHM
Monochrome	1.147μm
Color	1.155μm

3.2 Stent surface 3D measurement

As mentioned in the former subsection, a color camera allows obtaining 3D topographies with very similar vertical and lateral resolution as with a monochrome camera. We have developed the algorithms to perform a Z scan at 50fps with 2 Million pixel images; for each pixel we then calculate the envelope of the correlogram using the 5-point PSI algorithm proposed by Hariharan and detect its maximum to obtain the 3D topography[13]. Figure 4a shows the image of a strut defect appearing dark due to its local slope and the bright field objective's NA. Figure 4b shows the interferogram of this defect obtained with a Mirau interferometric objective. Finally, figure 4c shows the 3D topography after the CSI measurement, which allows the characterization of the defect, in this case a tip of 7 micrometers in height.

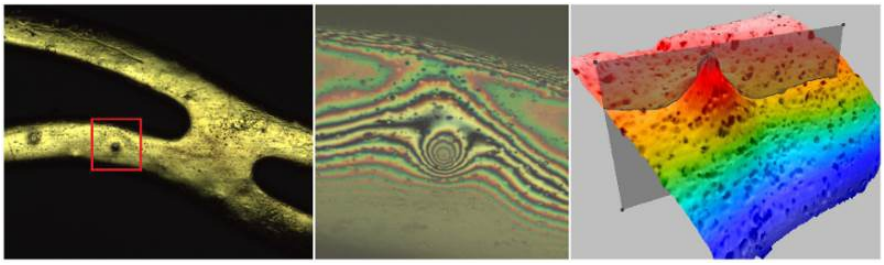

a b c

Figure 4. (a) Ambiguous defect (hole-bump), (b) Interferometric fringes, (c) 3D shape, tip is 7um in height.

4. COATING THICKNESS MEASUREMENT

In contrast with surface texture that can be measured both with contact and non-contact techniques, coating thickness cannot be measured by contact means, at least in a non-destructive approach. When the coating material is semi-transparent, it is possible to measure through the layer to the substrate using an optical technique.

Spectroscopic reflectometry is the conventional technique to perform optical non-contact coating thickness measurements. It consists of a single point technique that is based on the measurement of light reflected from the surfaces or interfaces of different layers on a substrate, and measures the average thickness value corresponding to a small area of the coating. To achieve higher lateral resolution, the fiber of the spectrometer can be connected to a microscope, thus by scanning the spot on the surface of the sample, a 3D map of the layer thickness can be recovered. However, due to the substrate roughness and the coating non-homogeneity, spectroscopic reflectometry performance is limited in many samples.

The alternative is using an optical profiler to characterize the upper and lower interfaces. Optical thickness profiling makes possible to evaluate the thickness at every point of the surface. By doing so, variations in thickness and

uniformity across an area up to several mm^2 can be highlighted. Interferometric and confocal techniques can be used to perform this type of measurement, giving the most comprehensive view of a coating. This is, in many applications, better than measurements made with other instruments that only measure a single average thickness value that will provide a very poor assessment of thickness variations and the uniformity of the coating and substrate surface.

One drawback of optical profiling techniques is that, although measurement of multilayer structures is theoretically possible, in practice the techniques are limited to the measurement of single layer samples. Another drawback is that sub-micrometric thickness measurements are not possible using the confocal technique and very difficult using interferometric techniques. However, stent coatings are usually single layer and in the range of some micrometers in thickness and therefore can be measured with optical profiling thickness measurement techniques. We have implemented and tested Confocal and Interferometric.

4.1 Confocal technique

In a confocal microscope, we obtain an image that suppresses the light falling outside from the depth of focus of the objective, while it preserves all the light that is in the depth of focus. This image is called an optical section. Three-dimensional measurements in a confocal microscope are achieved by scanning the surface through the depth of focus of the microscope and recording a series of optical sections. The height location for each pixel is calculated as the height corresponding to the optical section within all sections where this pixel achieves its highest intensity. The width of the optical section and thus the width of the axial response is proportional to the illumination wavelength and inversely to the NA. Therefore, the use of green light and high-NA objectives, typically 0.9 or 0.95 for dry objectives, gives nanometer level height resolution.

If the sample has a coating whose thickness (Th_M) is clearly greater than the width of the axial response, two peaks appear. One corresponds to the *air−coating* interface and the other to the *coating−substrate* interface. The distance between peaks is the measured (or apparent) thickness (Th_A), which increases with the thickness of the layer.

The measured separation of the peaks Th_A is very different from the real thickness Th_M of the coating as can be seen in Figure 4 because of two important factors: depth distortion due to the refractive index n of the medium and the spherical aberration caused by focusing with high NA optics through a refractive medium.

If the refractive index of the layer and the optical properties of the system, such as light source and objective NA, are known, the real thickness value Th_M can be determined[14]. For NAs lower than 0.45 it is as easy as using a simple correction factor based on a geometric model.

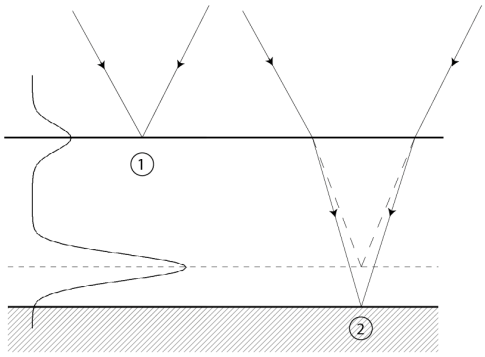

Figure 4. Axial response of a confocal microscope focusing on top (point 1) of the coating layer, and to the substrate (point 2). Focusing on the substrate appears to be closer to the air-coating interface due to focusing through a transparent media.

The theoretical thickness limit that can be measured is related to the numerical aperture of the microscope objective, which determines the width of the peak in the axial response and therefore determines the minimum necessary separation between the two peaks in order to be resolved. However, the separation between them corresponding to the two layer interfaces, which is always smaller than the real thickness, not only depends on the thickness of the layer but also on the optical properties of the material. This limits the ability of the confocal technique to measure thin films and is the opposite to what occurs with the CSI technique, where the separation between the envelope peaks is larger than the real thickness.

In our setup, the width of the axial response when the highest possible NA, 0.95 for dry objectives, and an illumination wavelength of 550nm are used is about 0.75µm, making the minimum resolvable optical layer thickness to 1.5µm. With respect to stent coatings, most of them are in the order of some micrometers in thickness, therefore confocal technique is theoretically suitable for this application.

We have applied this technique to a coated stent thickness measurement. Due to the roughness of the substrate and of the coating itself, a lot of noise appears on the interface due to a focusing effect produced by the outer layer, making confocal technique limited for such sample (Figure 5).

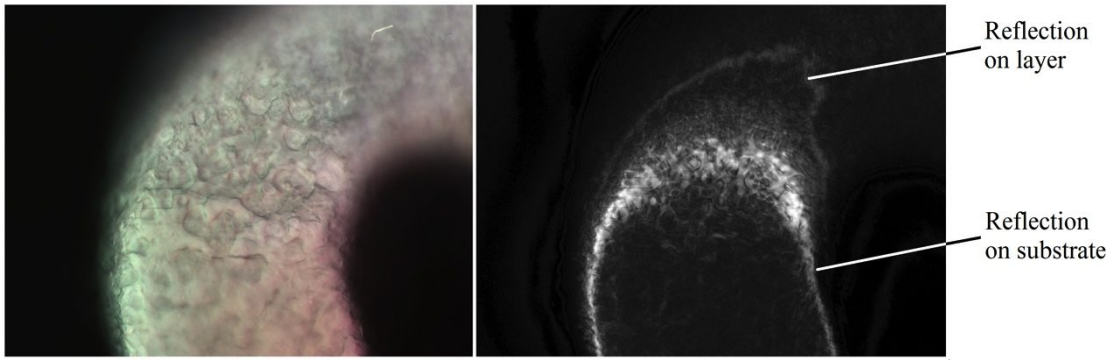

Figure 5. Image of a 40µm coating thickness coated stent, taken with a 50X NA0.8 microscope objective. (a) Color screenshot, (b) confocal image.

4.2 Coherence Scanning Interferometry (CSI)

Coating films can also be measured with interferometry. As opposed to the confocal technique, the interference pattern on the substrate appears deeper than its real location, due to an optical path difference of the rays travelling through the air inside the objective and the ones travelling through the coating (Figure 6). This effect causes the two interference signals to be more separated than the peaks on the confocal axial response, making possible to measure thinner layers of down to 1 micron approximately. Nevertheless, due to the focusing effect of the coating described in the confocal technique subsection, the substrate image is shifted closer to the *air-coating* interface, plunging the interferences contrast. To minimize it, lower numerical aperture objectives are desirable, making possible to measure thicker coatings (up to 30 microns with a 10X objective) with the substrate image still inside the objective depth of field.

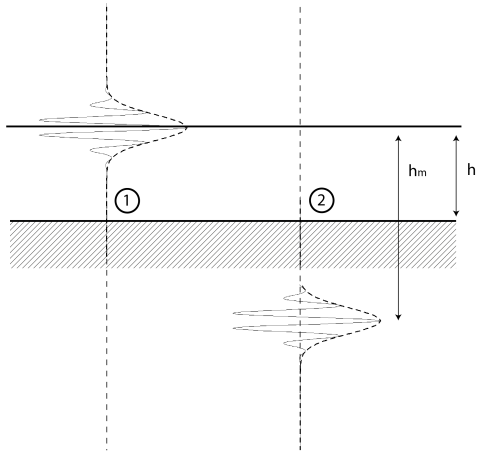

Figure 6. Correlograms on the *air-coating* interface (1) and the *coating-substrate* interface (2). The location of the second interference pattern appears deeper than the location of the *coating-substrate* interface.

Using an interference microscope for the measurement of stent coatings has the benefit of being able to measure a large area within a field of view of a low magnification objective maintaining the same height resolution.

According to the literature we make a Z scan at such a speed that allows us to grab images every λ/8 distance in height. As regards to signal processing, we obtain the envelope of the correlogram with a 5-point correlation kernel and we separate the two peaks of the correlogram envelop to process the two interfaces independently. Our splitting consists of using Otsu algorithm[15], which was developed for image segmentation. The apparent coating thickness is calculated as the difference between the two interfaces and the real thickness Th_M is obtained by dividing the apparent thickness Th_A by the refractive index n of the coating material.

4.3 Areal coating thickness measurement

The measurement of the stent coating thickness is performed on a surface which is not flat. Geometrically, the coating thickness depends on the observation angle and on the surface slope. In a stent with a uniform coating, measured thickness Th_M increases with the slope, in other words, as the observation point separates from the stent apex (Figure 7).

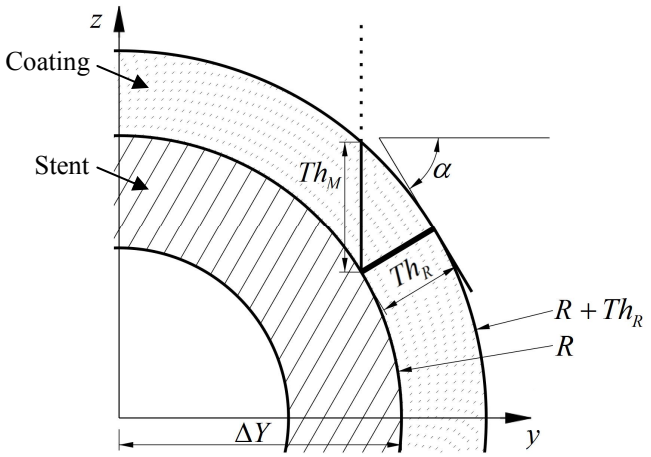

Figure 7. Schematic of an axial section of a coated stent with radius R and coating thickness Th_R. Thickness is being measured a certain distance ΔY apart from the stent apex thus obtaining a projected width (Th_M). α is the angle corresponding to the slope of the surface at the measuring point.

The correction model that we propose consists of finding the stent apex position, which can be obtained through a circular fitting, in order to determine the theoretical surface slope. Finally, with the following trigonometric equation the corrected thickness Th_R is obtained:

$$Th_R = \frac{Th_M}{R}\sqrt{R^2 - \Delta Y^2} \tag{1}$$

This model relies on a known stent diameter, which is common information in a stent inspection process as all the samples of the same kind come from the same tube, or it can even be easily measured. Nevertheless, we also propose a correction model based on the measuring point local slope, taking advance that we have already measured the 3D topography of the *air-coating* interface. Corrected thickness based on the local slope Th_{RS} is obtained by this simple equation:

$$Th_{RS} = Th_M \cos(\alpha) \tag{2}$$

Hence, in order to evaluate these correction methods we have recovered a stent with a sirolimus coating with refractive index n=1.49 and about 40μm thickness. We have performed a measurement in 3 different points of the surface, one centered with the optical axis and two well apart from it (Figure 8a and d). Afterwards, those two points aside from the center have been measured again but perpendicular to the optical axis (Figure 8b, e and c, f respectively) to evaluate the difference.

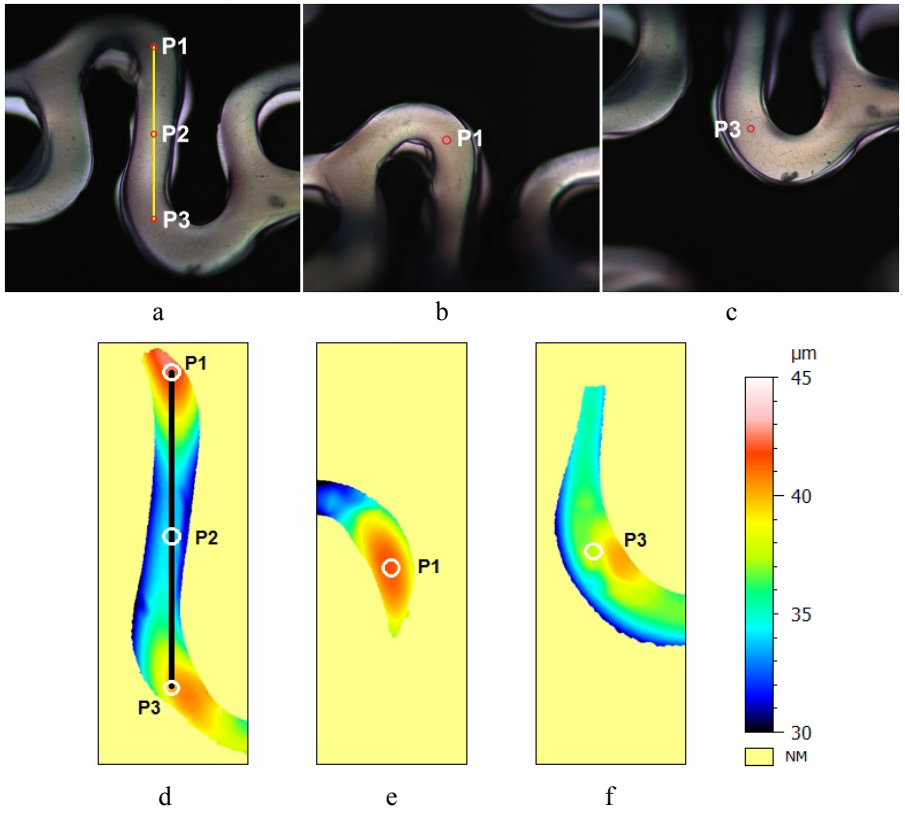

Figure 8. Thickness measurement of a sirolimus coating onto a Ø2mm stent. (a) Location of the measuring points perpendicular (P2) and non-perpendicular (P1 and P3) to the optical axis, (b) and (c) location of the points P1 and P3 centered with the optical axis. (d), (e) and (f) Topographies of the coating thickness corresponding to (a), (b) and (c).

The coating profiles section corresponding to Figure 8d are presented in Figure 9a. S1 corresponds to the *air-coating* interface and S2 to the *substrate-coating* interface. By subtracting both profiles and correcting the apparent thickness using the index of refraction we obtain the thickness profile Th_M and corrected Th_{RS} which appear in Figure 9b. Thickness error profile (differences between Th_R and Th_M) is shown in Figure 9c.

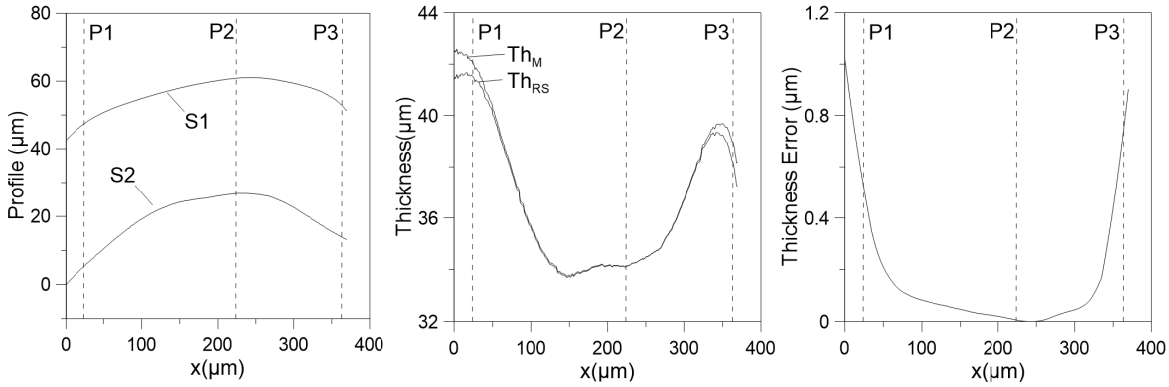

Figure 9. (a) Height profiles of the *air-cotaing* and *coating-substrate* interfaces, (b) subtraction of both profiles taking into account refraction index, obtaining Th_M and with the corrected model Th_{RS}, (c) measurement error between Th_M and Th_{RS}.

Finally, we have compared the thickness measurements in P1 and P3 from Figure 8d and Figure 8e and f. We have observed that the correction model from Eq.2 achieves very similar results to the perpendicular measurements:

Table 2. Results and comparison of the 3D thickness measurement when the measuring point is perpendicular and when the same point has a local slope versus the corrected model.

Point	Single 3D measurement (Figure 8d)	Perpendicular measurement (Figure 8e and f)	Corrected value from Figure 8d with Eq.3
P1	42.49µm	41.50µm	41.55µm
P2	33.96µm	33.96µm	33.96µm
P3	40.18µm	39.47µm	39.35µm

5. EXTENDED DEPTH OF FIELD

A crucial aspect of a stent visual inspection system is to be able to produce high quality, crystal clear images. Due to the usage of high magnification and NA objectives, their depth of field is limited to few microns, thus making only part of the stent image on focus. This effect is even more noticeable when inspecting sidewalls, where features appear in a range of several hundred microns depending on the field of view and on the stent dimensions. In order to get fully focused images, especially in the sidewalls, we have implemented an extended depth of field (EDF) or focus stacking algorithm. This technique obtains fully focused images by scanning along the Z axis, taking advance that the system already has a focus scan stage.

5.1 Algorithm determination

Although there are many computational techniques that determine the best focused plane for every pixel, most of them are texture-detection based. The most advanced are based on a multiresolution analysis[16]. In our particular case, only a small part of the image contains information (the struts) and the rest of the field of view is a constant background (Figure 10a), which can cause some of those algorithms to add noise into those invariant regions. Furthermore, most of the stents are polished and their surfaces have not much sharpness, making some techniques limited for this application. We have tested two image processing approaches which do not suffer from unfluctuating backgrounds. The first one consists of a 5x5 kernel Laplacian filter, the other one consists of a variance determination in a window of the same size (Eq.3):

$$Var(X) = \frac{1}{N}\sum_{i=1}^{N}\left(x_i - \frac{1}{N}\sum_{i=1}^{N}x_i\right)^2 \tag{3}$$

Where X corresponds to the variance in a given pixel, N to the amount of pixels in the window, in our case 25, and x_i to the intensity value of each pixel in the window.

Accordingly, we have observed that each algorithm has its particularities. Although it is true that none creates artifacts in the background, the variance approach adds some noise onto the strut (Figure 10b), while some of the most minuscule details of the image are unnoticed when using the Laplacian (Figure 10c).

a b c

Figure 10. (a) Screenshot of a stent strut, being the sidewall not fully focused. Generation of the EDF image by (b) variance algorithm, (c) Laplacian filter.

We have ascertained that a fusion between both algorithms, weighting with a 70% the Laplacian the and with a 30% the variance, we can obtain the best results for this kind of samples. Moreover, we have explored two different stack recovery methods: maximum projection and weighted intensity. We have observed that weighted intensity is the best

recovery method for our samples that are in general glossy (Figure 11a), where maximum projection produces uneven and unrealistic images (Figure 11b).

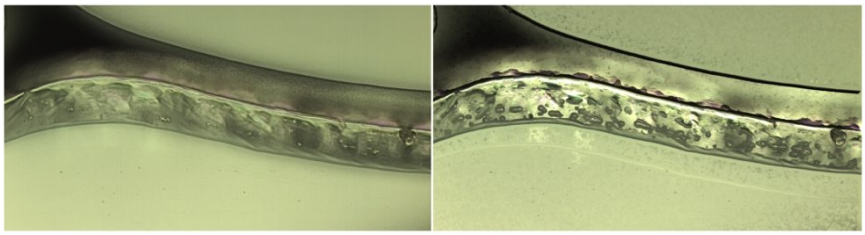

a b

Figure 11. Final EDF image combining the Laplacian filter and the variance calculation, comparing two different stack recovery methods: (a) weighted intensity, (b) maximum projection.

5.2 Real time image processing

Apart from the ability to produce EDF images from the stent struts, above all in sidewalls, another relevant concern is to generate them rapidly, if not instantly, One of the first aspects to improve is to boost the double calculation loop of Eq.3, which has been extended in two separated summations, being it computationally more agile since it has a single multiplication per window position (Eq.4):

$$Var(X) = \frac{1}{N}\left(\sum_{i=1}^{N} (x_i)^2 - \left(\sum_{i=1}^{N} (x_i) \right)^2 \right) \tag{4}$$

Our camera provides 2 Million pixel images at 50 fps. Overall, we have determined that every image consumes around 60ms to be processed using some of the most modern and powerful microprocessors. This makes that after image acquisition at 50 fps, the user needs to wait for the calculation to end, independently of the number of images recorded. Specifically, the waiting time is equivalent to the double the scanning time.

Algorithms described formerly are suitable for parallel computing, as they work with small pieces of the overall dataset. That has led us to propose a GPU implementation to reduce the execution time. Since both algorithms read every single pixel several times, the use of the GPU shared memory is advisable, as it has much faster access than the global memory. However, shared memory has a limited capacity. In our conditions, we have divided the images into blocks of 16x16 pixels, adding two acron pixels to each side so as to use the 5x5 kernels. Final block dimension is 20x20 pixels. Obtained results report a 4.3x speed increase with respect to the classical CPU implementation (Figure 12). Execution time plunges to less than 15ms per image, thus processing the data in real-time and supplying the user with the final result just after the Z scan is completed.

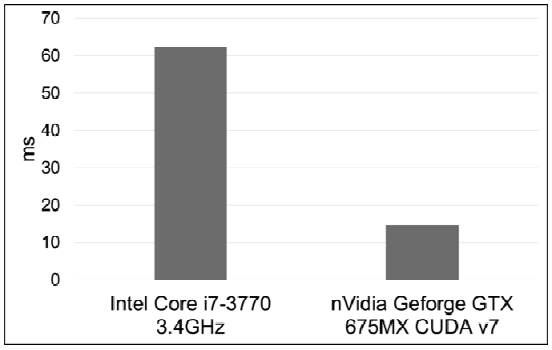

Figure 12. EDF processing time per 2Mpix image. While CPU processes each image in about 62ms, same algorithm is executed in GPU in less than 15ms, thus achieving a performance increase of 4.3x.

6. CONCLUSIONS

In this paper, a 2D and 3D optical stent inspection system has been presented. It consists of an epi and back illumination, high numerical aperture microscope objectives, together with a rotational stage, and a 2 Million pixel CMOS color camera that can behave both as area-scan and line-scan, so as to acquire 2D unrolled images from the stent. 3D capabilities are achieved by adding additional components such as a Z scanner to perform coherence scanning interferometry (CSI) and a second, structured illumination branch, to implement the confocal technique. An additional 2D mode has been implemented taking advantage of the Z scanner: fully focused images (extended depth of field, EDF) of a stent region. Using these 2D and 3D modes, form, texture and defects from the stent surfaces can be evaluated.

As regards to coating thickness analysis, we have demonstrated that neither confocal nor spectroscopic reflectometry are optimum for this application, due to substrate roughness and coating non-homogeneity. Nevertheless, interferometry is fully suitable and can recover the thickness topography precisely. Stent cylindrical shape plays a role on this measurement, due to the thickness projection of the layer. Two geometric correction methods are proposed, one based on the stent diameter and the inspection position with respect to the apex and another one based on the local slope. We have validated both correction methods by measuring perpendicularly in the areas formerly tilted and corrected.

As regards to the need of high quality 2D imaging in sidewalls, we can overcome the limitation in depth of field of high NA microscope images by implementing an EDF image algorithm. It consists of a Laplacian filter and a variance calculation, which is tolerant to invariable background and to polished surfaces, as are most stents. For this kind of samples, weighted intensity stack recovery approach fits better than maximum projection. Finally, in order to produce EDF results in real-time, we have implemented said algorithms for a GPU execution, providing a 4.3x speed increase with respect to CPU processing.

REFERENCES

[1] Katona, B., et al., "Chemical etching of nitinol stents," Acta of Bioengineering and Biomechanics 15(4) (2013).
[2] Muramatsu, T., et al., "Avances en el tratamiento mediante intervención coronaria percutánea: el stent del futuro," Rev Esp Cardiol. 66(6), 483-496 (2013).
[3] Abizaid, A., Ribamar, J., "New Drug-Eluting Stents. An overview on Biodegradable and Polymer-Free Next-Generation Stent Systems," Circ Cardiovasc Interv. 3, 384-393 (2010).
[4] Freifeld, D., "Repetitive inspection system with intelligent tools", US Patent 6,606,403 (2003).
[5] Maehringer-Kunz, E., et al., "Automatic inspection device for stents, and method of automatic inspection," PCT/EP2006/065814 (2006).
[6] Ibraheem, I., Binder, A., "An automated inspection system for stents," The International Journal of Advanced Manufacturing Technology 47**,** 945-951 (2009).
[7] Jin, J., "Automatic stent inspection system," US Patent 2010/0309307 (2010).
[8] Bermudez, C., Laguarta, F., Cadevall, C., Matilla, A., Ibañez, I., and Artigas, R., "Novel Stent Optical Inspection System," Imaging and Applied Optics 2016, OSA Technical Digest (online), Optical Society of America, paper AITh2B.3 [doi:10.1364/AIO.2016.AITh2B.3] (2016).
[9] Laguarta, F., Bermudez, C., Artigas, R., Cadevall, C., "Device and method for optically inspecting and analysing stent-like objects," PCT/EP2013/078085 (2013).
[10] Artigas, R., Pinto, A.; Laguarta, F., "Three-dimensional micromeasurements on smooth and rough surfaces with a new confocal optical profiler," Proc. SPIE 3824, 93 [doi:10.1117/12.364243] (1999).
[11] de Groot, P., "Coherence Scanning Interferometry," [Optical measurement of surface topography], Springer, Berlin, 187-206 (2011).
[12] Guo, T., Gu, Y., Chen, J., Fu, X., Hu, X.; "Surface topography measurement based on color images processing in white light interferometry," Proc. SPIE 9525, 952511 [doi:10.1117/12.2184558] (2015).
[13] Larkin, K.G.; "Efficient nonlinear algorithm for envelope detection in white light interferometry," J. Opt. Soc. Am. A, Vol. 13, No. 4 (1996).
[14] Cadevall C., Artigas R., Laguarta F.; "Development of confocal-based techniques for shape measurements on structured surfaces containing dissimilar materials," Proc. SPIE 5144, 206-217 (2003).
[15] Chang, S.P., Xie, T.B., Sun, Y.L., "Measurement of Transparent Film Using Vertical Scanning White-Light Interferometry," Journal of Physics: Conference Series 48, 1063-1067 [doi:10.1088/1742-6596/48/1/198] (2006).
[16] Aguet, F., Van De Ville, D., Unser, M., "Model-Based 2.5-D Deconvolution for Extended Depht of Field in Brightfield Microscopy," IEEE Transactions on Image Processing, Vol. 17, No. 7 (2008).